JACS
JOURNAL OF THE AMERICAN CHEMICAL SOCIETY
pubs.acs.org/JACS
Article

Atroposelective Negishi Coupling Optimization Guided by Multivariate Linear Regression Analysis: Asymmetric Synthesis of KRAS G12C Covalent Inhibitor GDC-6036

Jie Xu, Samantha Grosslight, Kyle A. Mack, Sierra C. Nguyen, Kyle Clagg, Ngiap-Kie Lim, Jacob C. Timmerman, Jeff Shen, Nicholas A. White, Lauren E. Sirois, Chong Han, Haiming Zhang,* Matthew S. Sigman,* and Francis Gosselin

Cite This: J. Am. Chem. Soc. 2022, 144, 20955−20963
Read Online
ACCESS | Metrics & More | Article Recommendations | Supporting Information

ABSTRACT: An efficient asymmetric synthesis of a potent KRAS G12C covalent inhibitor, GDC-6036 (**1**), is reported. The synthesis features a highly atroposelective Negishi coupling to construct the key C−C bond between two highly functionalized pyridine and quinazoline moieties by employing a Pd/Walphos catalytic system. Statistical modeling by comparing computational descriptors of a range of Walphos chiral bisphosphine ligands to a training set of experimental results was used to inform the selection of the best ligand, **W057-2**, which afforded the desired Negishi coupling product (R_a)-**3** in excellent selectivity. A subsequent telescoped reaction sequence of alkoxylation, global deprotection, and acrylamide formation, followed by a final adipate salt formation, furnished GDC-6036 (**1**) in 40% overall yield from starting materials pyridine **5** and quinazoline **6**.

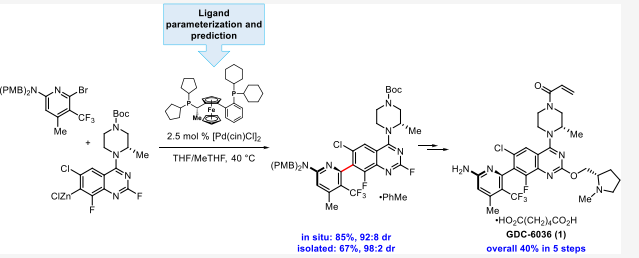

INTRODUCTION

KRAS is widely considered as one of the most commonly mutated oncogenes and actively pursued anticancer targets and has attracted tremendous attention in research oncology.[1−4] However, discovering potent and selective KRAS inhibitors has remained one of the ultimate challenges of cancer research in the last decades.[5] Until recently, by targeting a specific G12C mutation via an irreversible covalent inhibition strategy, groundbreaking progress was made that led the first KRAS inhibitors to reach the clinical stage to treat patients (Figure 1).[6−12]

Genentech has had a long-standing interest in the pursuit of KRAS G12C inhibitors to address unmet medical needs. GDC-6036 (**1**), a highly potent and selective KRAS G12C irreversible covalent inhibitor, has emerged from our research pipeline after extensive structure−activity relationship (SAR) studies and is currently in late-stage clinical development to treat a wide spectrum of cancers (Figure 1).[11]

Structurally, GDC-6036 (**1**) features a highly reactive acrylamide warhead and two densely functionalized quinazoline and pyridine heterocycles. Uniquely, GDC-6036 (**1**) contains a sterically hindered, rotationally restricted C−C bond between the two heterocyclic moieties and is a stereodefined single atropisomer with calculated and measured rotation barriers of 28.2 and 30.1 kcal/mol, respectively.

Since the first report of atropisomeric compounds by Christie and Kenner in 1922,[13] the synthesis and application

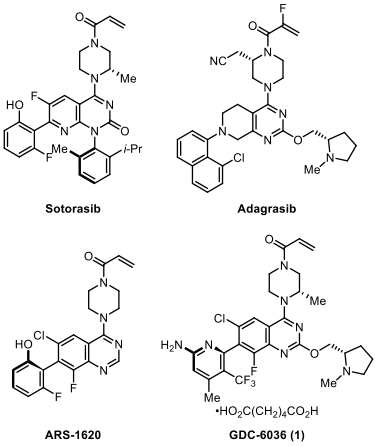

Figure 1. Structures of leading KRAS G12C covalent inhibitors and GDC-6036 (**1**).

Received: September 16, 2022
Published: November 3, 2022

of these compounds in catalysis, natural products, and pharmaceutics have been extensively studied with significant advances reported during the last decades.[14−19] However, highly atroposelective C−C bond formations, especially in the context of complex and highly substituted nitrogen-rich heterocycles, remain elusive to date (Scheme 1A).[20−25]

Scheme 1. Formation of Nitrogen-Rich Heterocycles or Biaryls by Atroposeletive Suzuki−Miyaura or Negishi Coupling

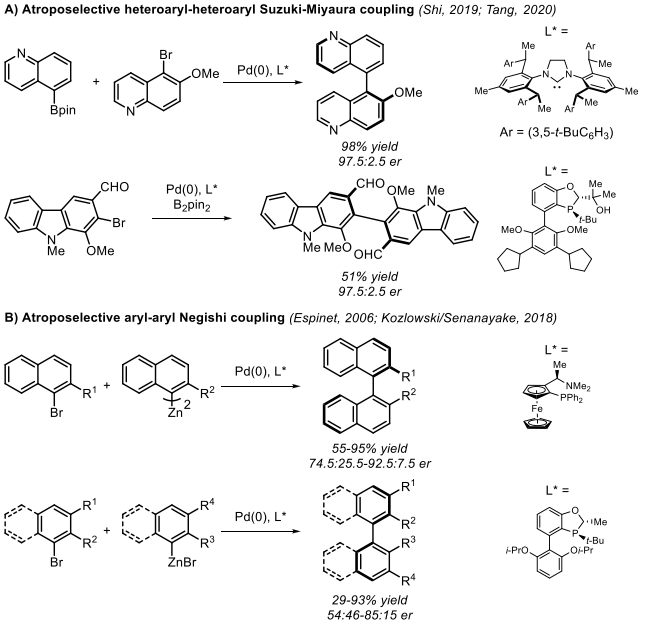

Among the very limited number of reported examples, most involved atroposelective formation of a heterocycle containing noncoordinating nitrogen such as indole or carbazole. Similarly, atroposelective C−C bond formations via Negishi coupling are rare in the literature.[26−28] The few known examples focus on the synthesis of substituted biaryls, specifically binaphthalenes and biphenyls, with limited scope and moderate atroposelectivities (Scheme 1B).

In support of our clinical and commercial development of GDC-6036 (**1**), we sought to develop an efficient atroposelective synthesis of the active pharmaceutical ingredient (API). Herein we report a viable first-generation synthesis of GDC-6036 (**1**) featuring a highly atroposelective Negishi coupling[29,30] catalyzed by a Pd/Walphos[31,32] system. The identification of the most effective ligand was informed by combining high-throughput experimentation (HTE) with statistical modeling of the reaction outputs using multivariate linear regression (MLR) analysis of computationally derived bisphosphine structural descriptors.[33]

RESULTS AND DISCUSSION

We envisioned that GDC-6036 (**1**) could be assembled by a global deprotection of an advanced intermediate **2** followed by an acrylamide warhead installation. Compound **2** could be synthesized by an alkoxylation of intermediate (R_a)-**3** with alcohol **4** via an S_NAr reaction of the heteroaryl fluoride. Intermediate (R_a)-**3** then could be derived from a catalyst-controlled diastereoselective formation of the desired atropisomer via a metal-catalyzed cross-coupling of bromopyridine **5** and quinazoline **6b** (Scheme 2). This key reaction would not only set the chiral axis but also combine two densely functionalized, nitrogen-rich components.

Scheme 2. Retrosynthesis of GDC-6036 (1)

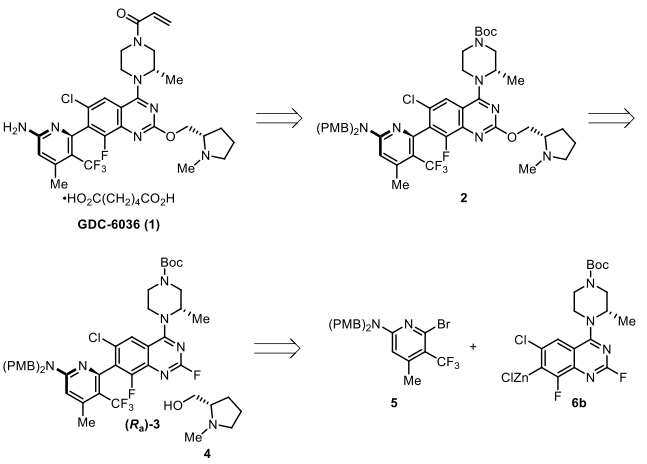

Our preliminary experiments indicated that the Suzuki−Miyaura reaction was not feasible, as the quinazoline boronic acid readily underwent deleterious protodeborylation, and the optimally reactive combination would entail formation of a quinazoline organozinc species.[34] Thus, treating quinazoline **6** with *i*-PrMgCl·LiCl at −78 °C readily led to metal−halogen exchange to afford organomagnesium intermediate **6a**. Transmetalation of **6a** with $ZnCl_2$ produced the corresponding stable organozinc intermediate **6b**. We then conducted an HTE exploration of the Negishi coupling of bromopyridine **5** and organozinc **6b** by employing 10 mol % achiral phosphine ligand based palladium precatalysts, expecting to form the key C−C bond in the Negishi product **3**, albeit in a non-stereoselective fashion (see Supporting Information). Gratifyingly, while various mono- and bisphosphine ligand based palladium precatalysts afforded good conversion and assay yield of the Negishi product **3**, $PdCl_2(PPh_3)_2$ was identified as the best catalyst by HTE. The optimized Negishi coupling employed 4 mol % $PdCl_2(PPh_3)_2$ as the catalyst and 1.2 equiv of **6b** and was subsequently validated at 5.0 g (10 mmol) scale. The reaction produced 85% assay yield of the Negishi product **3** as a 50:50 diastereomeric mixture, which indicates that the existing piperazine stereocenter does not transfer its stereochemical information to the axis of chirality under these reaction conditions. Product **3** was isolated in 58% yield after chromatographic purification and crystallization in MeOH (Scheme 3).

Encouraged by the results of this Negishi coupling, we then set out to examine the atroposelective Negishi coupling of bromopyridine **5** and quinazoline organozinc species **6b** by employing $Pd(OAc)_2$ and chiral ligands in a subsequent HTE

Scheme 3. Non-stereoselective Negishi Coupling to Form 3

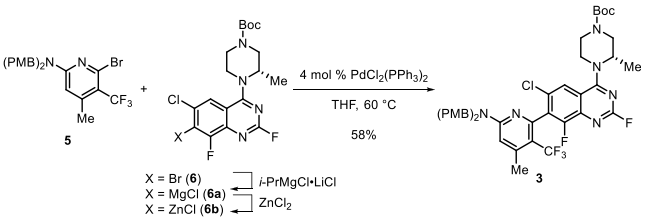

https://doi.org/10.1021/jacs.2c09917
J. Am. Chem. Soc. 2022, 144, 20955−20963

campaign (Scheme 4 and Supporting Information). In spite of the broad range of chiral ligands (**L1**−**L24**) examined, most

Scheme 4. Initial HTE of Atroposelective Negishi Coupling

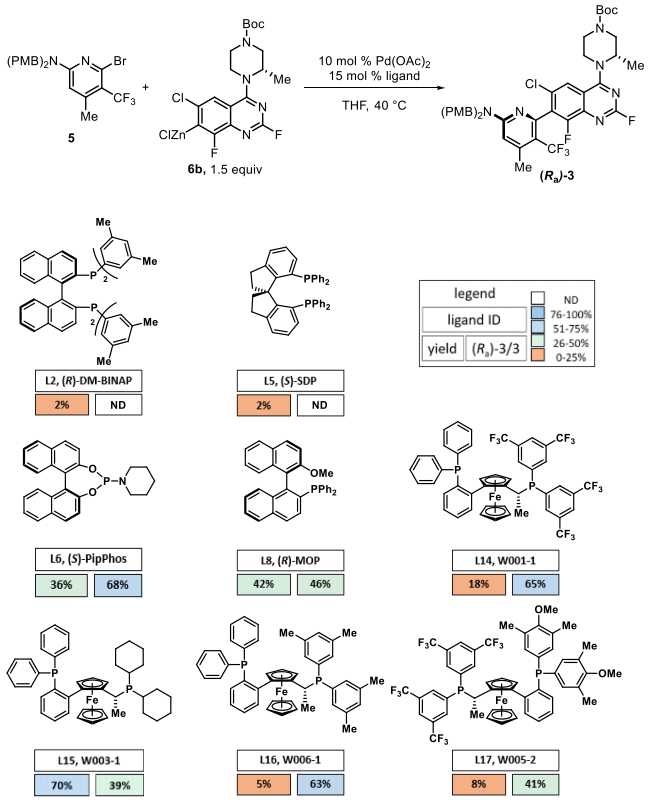

gave no product (Supporting Information). However, a number of privileged ligands, especially those from the Walphos ferrocenyl bisphosphine family **L14**, **L15**, **L16**, and **L17**, consistently provided promising reactivity and atroposelectivity as determined by HPLC analysis (Scheme 4). Intriguingly, Walphos **L15** (**W003-1**) gave the highest assay yield of the product **3** (70%) as a 39:61 diastereomeric mixture favoring the undesired atropisomer. While simultaneously evaluating other classes of chiral ligands to improve the atroposelectivity of the Negishi reaction, we undertook a focused investigation of the structure−selectivity relationship (SSR)[35] of the Walphos family of ligands in the Negishi reaction to ultimately improve the observed selectivity.

Our Walphos-focused ligand optimization commenced with the validation of **W003-1** under slightly modified HTE conditions employing 2.5 mol % palladium(π-cinnamyl) chloride dimer [Pd(cin)Cl]$_2$ and 5 mol % ligand at 40 °C (Table 1). Consistent with the HTE results, the reaction readily produced the Negishi product **3** in 84% assay yield and 39:61 atroposelectivity favoring the undesired atropisomer (Table 1, entry 1). A reaction employing enantiomeric **W003-2** generated a similar profile but favored the desired atropisomer (R_a)-**3** with a reversed 61:39 atroposelectivity, confirming again that the distant stereocenter on the piperazine ring does not impact the atroposelectivity (Table 1, entry 2). Decreasing the electron density on the right-hand phosphine P_R in **W002-1** and **W001-1** significantly reduced the conversion of the reaction (Table 1, entries 3, 4), albeit favoring the desired atropisomer (R_a)-**3**. Increasing the steric bulk on P_R by replacing dicyclohexyl with a dinorbornyl group

Table 1. Optimization of Negishi Coupling Employing Walphos Ligands

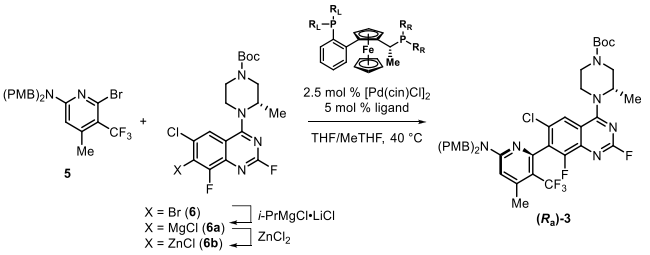

entry[a]	Walphos	conv (%)[b]	**3** (A%)[b,c]	dr[b]
1	**W003-1**	100	75 (84)[d]	39:61
2	**W003-2**	100	78	61:39
3	**W002-1**	17	8	60:40
4	**W001-1**	10	7	69:31
5	**W022-1**	100	84 (85)[d]	78:22
6	**W012-1**	43	40	74:26
7	**W039-1**	85	64	15:85
8	**W029-1**	6	4	
9	**W030-1**	<5		

[a]Reaction conditions: **6** (289 mg, 150 mol %) in THF (1.2 mL), *i*-PrMgCl·LiCl (0.48 mL, 1.3 M in THF, 155 mol %), −78 °C; $ZnCl_2$ (0.33 mL, 1.9 M in 2-MeTHF, 155 mol %), −78 → 20 °C; then **5** (200 mg, 0.404 mmol), [Pd(cin)Cl]$_2$ (5.5 mg, 2.5 mol %), Walphos ligand (5 mol %) in THF (1.2 mL), 40 °C, 18 h. [b]Determined by HPLC analysis. [c]The protodebromination product of **6** after quench was not integrated. [d]Assay yields are indicated in parentheses, determined by quantitative HPLC analysis.

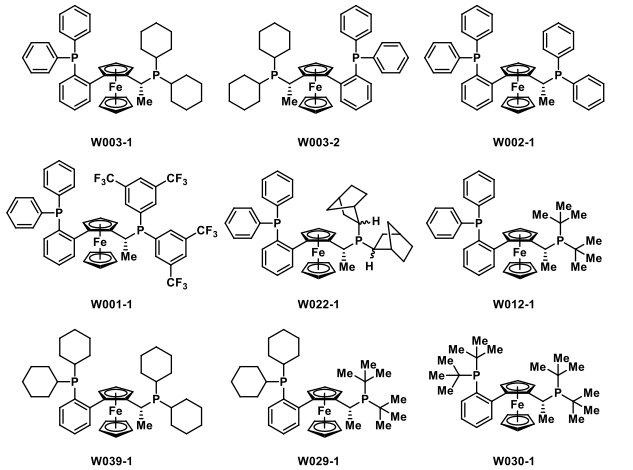

(**W022-1**) restored the reactivity and also favored the formation of the desired atropisomer (R_a)-**3** in 78:22 dr (Table 1, entry 5). Further increasing the size on P_R with a di-*tert*-butyl group had a negative impact on the conversion, while the atroposelectivity was largely maintained (74:26, Table 1, entry 6). Relatively high reactivity and atroposelectivity were realized when **W039-1**, having a dicyclohexyl group on both P_L and P_R, was employed as the ligand. The reaction afforded 85% conversion and 15:85 atroposelectivity favoring the undesired atropisomer (Table 1, entry 7). Substituting the dicyclohexyl group on P_R or both P_R and P_L with the bulkier di-*tert*-butyl group (**W029-1** or **W030-1**) essentially shut down the reaction (Table 1, entries 8, 9).

Preliminary trends from this optimization work indicated that electron-rich groups on both P_R and P_L facilitated the reaction, while excessively sterically bulky substituents (e.g., *t*-

https://doi.org/10.1021/jacs.2c09917
J. Am. Chem. Soc. 2022, 144, 20955−20963

Bu) had the opposite impact. However, we were unable to intuitively identify a clear trend of atroposelectivity versus ligand structure. In consideration of the synthetic challenges associated with performing structure−selectivity relationship studies on the Walphos ligands[31,32] and the lack of a clear direction for improving the atroposelectivity of the Negishi coupling, we sought to utilize data science tools, namely, multivariate linear regression analysis.[33] If successful, this strategy would provide an interpretable and predictive model by relating DFT structural features of the Walphos ligand structure to the experimentally measured atroposelectivity.

For the development of this predictive platform, we utilized a group of 11 Walphos ligands that were commercially available and diverse in their electronic and steric elements on both P_L and P_R (Scheme 5).[36] While the **W0xx-1** ligands do

Scheme 5. Training Set of Walphos Ligands for MLR Model Development

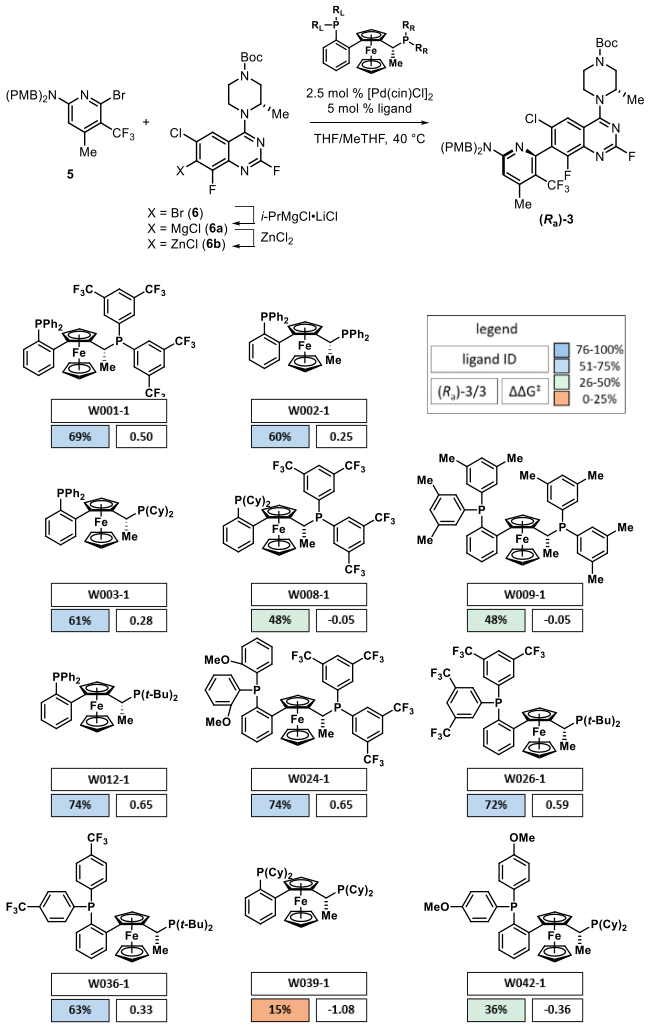

not consistently afford the preferred diastereomer (R_a)-**3**, we established that the desired product could be accessed by using the corresponding opposite Walphos enantiomer (**W0xx-2**). As such, we utilized a training set composed of only **W0xx-1** ligands for model development to provide predictions for untested Walphos (**W0xx-1**) ligands. Based upon these predictions, we could then choose the correct Walphos enantiomer to access the desired diastereomer (R_a)-**3**.

With an experimental training set in hand, we turned to the in-silico acquisition of molecular features for these Walphos ligands. When considering molecular features for collection, we elected to utilize $PdCl_2$ complexes for our calculations to mimic catalytically relevant species in solution for a Pd(0/II) mechanism. Density functional theory (DFT) optimization and subsequent single-point calculations were carried out on the $PdCl_2$·Walphos complexes for molecular feature acquisition (see Supporting Information for computational details). The molecular features collected include bond lengths, angles, Vbur, NBO charges, and bonding energies (see Supporting Information for a full list of molecular features).[37−42] Due to the nature of the Walphos ligand scaffold, the two phosphines are not identical. Consequently, parameters were collected corresponding to each phosphorus atom independently when appropriate (see Supporting Information). The variation between the two phosphines is further enhanced by the highly modular synthesis to access them, such that both phosphines are often functionalized independently.[31,32]

The extracted molecular features were regressed against the experimentally measured atroposelectivity utilizing a forward stepwise linear regression algorithm to produce a statistical correlation with terms describing both Walphos phosphines (Figure 2).[37] A three-term model composed of both steric and

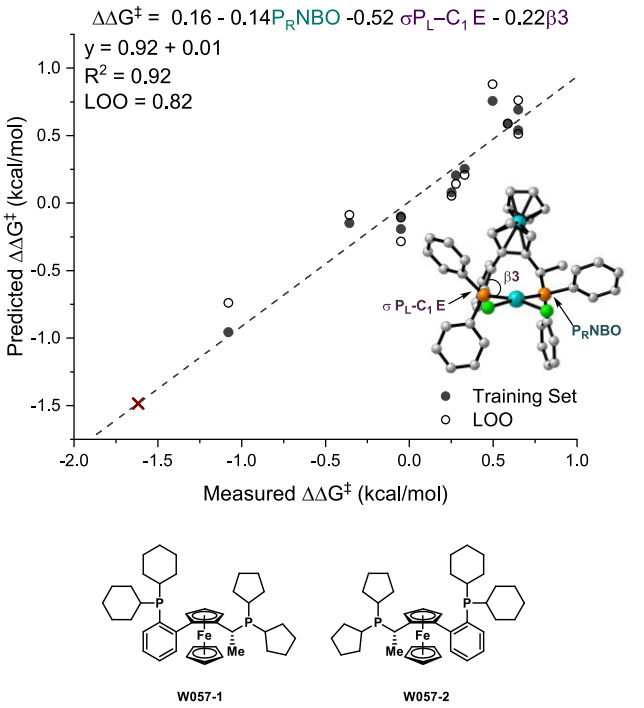

Figure 2. MLR model for atroposelective Negishi coupling reaction (maroon × = **W057-1**) and structures of **W057-1** and its enantiomer **W057-2**.

electronic molecular features was identified to describe the observed diastereoselectivity. Of these three molecular features, two describe the local environment around P_L and suggest that the observed diastereoselectivity may be influenced to a greater extent by the nature of P_L, whereas the modifications to P_R (described by the NBO charge of the phosphine) are less influential for selectivity. For P_L, the σ donation for the substituent to the phosphine is described by the σ bond energies (σP_L-C_1 E). Generally, Walphos ligands in

https://doi.org/10.1021/jacs.2c09917
J. Am. Chem. Soc. 2022, 144, 20955−20963

which P_L is substituted with alkyl substituents lead to more selective catalysts. The steric environment about P_L, described by the angle between palladium, P_L, and C_3 (carbon connecting P_L to the ferrocene framework) and labeled as the β3 angle, has less influence upon diastereoselectivity. With this model in hand, we sought to deploy it as a prediction platform to screen for Walphos ligands with improved diastereoselectivity. Upon virtual screening on untested Walphos ligands, we identified **W057-1** as a promising ligand with excellent predicted selectivity ($\Delta\Delta G^{\ddagger}_{pred}$ = −1.5 kcal/mol) for the undesired diastereomer. To access the desired diastereomer, we expected the enantiomeric **W057-2** ligand to exhibit a similar level of selectivity favoring the desired product (Figure 2). Gratifyingly, both **W057-1** and **W057-2** performed as predicted with **W057-2** $\Delta\Delta G^{\ddagger}_{exp}$ = +1.5 kcal/mol and **W057-1** $\Delta\Delta G^{\ddagger}_{exp}$ = −1.6 kcal/mol.

The performance of Walphos **W057-2** was demonstrated in the Negishi coupling reaction of bromopyridine **5** and 1.5 equiv of quinazoline organozinc **6b** employing 2.5 mol % $[Pd(cin)Cl]_2$ as the catalyst and 5 mol % of **W057-2** in THF/MeTHF at 40 °C, which resulted in a 85% assay yield of product **3** in 92:8 atroposelectivity (measured $\Delta\Delta G^{\ddagger}$ = −1.5 kcal/mol) favoring the desired product (R_a)-**3**. Further optimization led to the reduction of quinazoline organozinc **6b** to 1.3 equiv. The reaction was successfully demonstrated on a multigram scale of **5**, and the resulting product was crystallized as a toluene channel solvate in 67% yield and 98:2 diastereomeric ratio (Scheme 6). The structure of the Negishi product (R_a)-**3** was unambiguously established by X-ray crystallographic analysis (Figure 3).[43]

Scheme 6. Atroposelective Negishi Coupling Using Walphos W057-2 as the Ligand

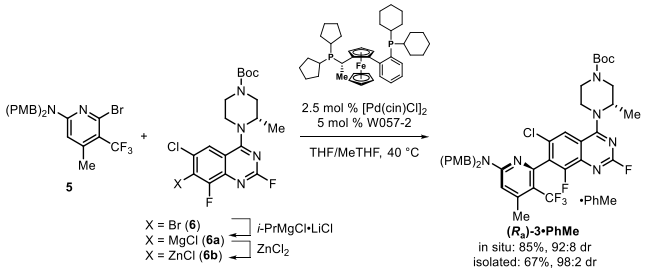

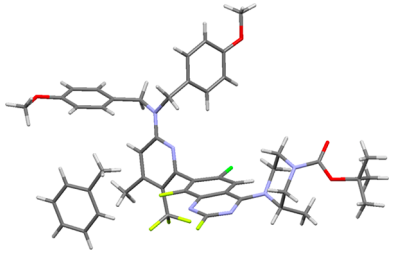

Figure 3. X-ray structure of (R_a)-**3**·PhMe.

We briefly evaluated the scope of this atroposelective Negishi coupling using ligand **W057-2** (Table 2). Due to the inherent sensitivity of axial chirality to temperature, the design and selection of substrates first required establishing the stability of the atropisomers to the reaction conditions (40 °C) (see Supporting Information). Furthermore, we sought to evaluate this method against heteroaromatics, a substrate class that has not been explored in most other atroposelective cross-coupling reactions. Additionally, an emphasis was on couplings with similar core features to those of (R_a)-**3** (Table 2). Unfortunately, we observed limited success using **W057-2** as the ligand for **7a**−**e**. For example, the Negishi coupling of bromopyridine **5** with truncated arylzinc reagents did not produce appreciable amounts of the desired products **7a**,**b** (Table 2, entries 1, 2). Additionally, the coupling of 2-bromo-3-isopropylpyridine with (2-chloro-6-fluorophenyl)zinc chloride afforded relatively low yield (25%) and modest selectivity (74:26) of the Negishi product **7c** (Table 2, entry 3). Electron-deficient 2-bromo-3-(trifluoromethyl)pyridine and 3-bromo-4-(trifluoromethyl)pyridine gave 59% and 16% yields of products **7d**,**e** in 60:40 and 79:21 enantiomeric ratios, respectively (Table 2, entries 4, 5).

Table 2. Scope of the Negishi Coupling Employing W057-2

Entry[a]	Product	Conv (%)[b]	Yield (%)[c]	*er*[b]
1	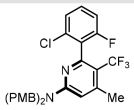 **7a**	12	3	88:12
2	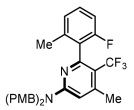 **7b**	24	8	75:25
3	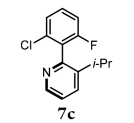 **7c**	37	25	74:26
4	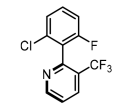 **7d**	72	59	60:40
5	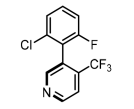 **7e**	31	16	79:21

[a]Representative conditions: 1-chloro-3-fluoro-2-iodobenzene (83.3 mg, 0.325 mmol, 130 mol %) in THF (0.28 mL), *i*-PrMgCl·LiCl (0.25 mL, 1.3 M in THF, 135 mol %), −78 °C; $ZnCl_2$ (0.18 mL, 1.9 M in 2-MeTHF, 135 mol %), −78 → 20 °C; then **5** (125 mg, 0.250 mmol), $[Pd(cin)Cl]_2$ (3.4 mg, 2.5 mol %), **W057-2** (8.3 mg, 5 mol %) in THF (0.28 mL), 40 °C, 18 h. [b]Determined by HPLC analysis. [c]Isolated yield.

The generally poor performance of **W057-2** as the ligand within the evaluated scope suggests that atroposelectivity is controlled by features of both coupling partners and the Walphos structure. This lack of generality is not altogether surprising, as the structural aspects of the coupling partners are likely to be matched to a particular ligand. Indeed, this has been observed by Kozlowski and Senanayake,[28] who demonstrated that by exchanging even a methyl for an ethyl group at the 2 and 2′ positions in their binaphthalene Negishi cross-coupling resulted in an attenuated atroposelectivity. This problem was further exacerbated by additional functionalization (e.g., methyl group installed at the 3 and 3′ positions). As such, we probed the question whether the MLR workflow could identify better ligands for several examples in the scope evaluation. To accomplish this, we subjected substrates **7c**−**e** to the atroposelective Negishi reaction using the training set of

https://doi.org/10.1021/jacs.2c09917
J. Am. Chem. Soc. 2022, 144, 20955−20963

Walphos ligands deployed for (R_a)-**3**.[44] Unsurprisingly, we were unable to find general statistical models for atroposelectivity and had varying degrees of success with model development (Figure 4). For example, the robust and

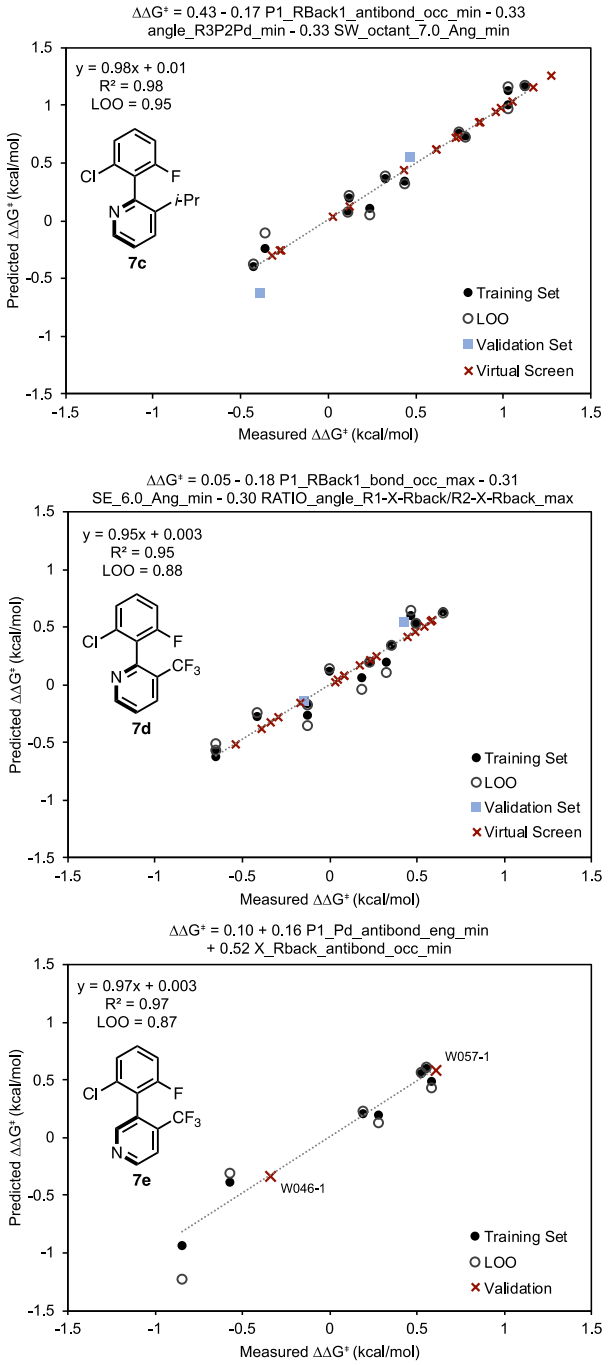

Figure 4. Models for **7c** (top), **7d** (middle), and **7e** (bottom).

predictive model for **7c** correctly identified a more selective ligand, **W052-1** (predicted $\Delta\Delta G^{\ddagger}$ = 1.3 kcal/mol), through virtual screening and was confirmed experimentally with a measured $\Delta\Delta G^{\ddagger}$ = 1.2 kcal/mol (Figure 4 and eq 1). Unlike **7c**, **7e** displayed poor reactivity within the Walphos training set, resulting in limited data for model development, and provided less than optimal predictions (**W057-1** predicted $\Delta\Delta G^{\ddagger}$ = +0.6 kcal/mol, **W057-2** measured $\Delta\Delta G^{\ddagger}$ = −0.5, **W046-1** predicted $\Delta\Delta G^{\ddagger}$ = −0.3 kcal/mol, measured $\Delta\Delta G^{\ddagger}$ =

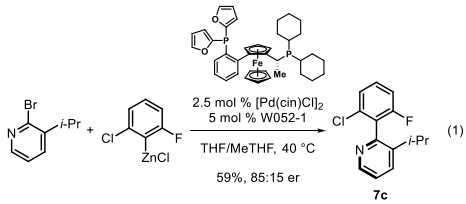

+0.6 kcal/mol (Figure 4). While moderate enantioselectivities were observed for **7d**, no better performing ligands were identified via virtual screening (Figure 4 middle). The best ligand, **W026-1**, was already included in the training set (74:26, $\Delta\Delta G^{\ddagger}$ = +0.65 kcal/mol). The extreme variation in both selectivity and reactivity within **7c**−**e** suggests that selective couplings are influenced by both coupling partners and the chiral environment created by the catalyst. As a consequence, we are exploring an in-depth investigation of the reaction scope of this atroposelective Negishi coupling to better understand the apparent complex substrate−selectivity relationships. With the key Negishi coupling product (R_a)-**3** in hand, a subsequent telescoped reaction sequence involving an alkoxylation of (R_a)-**3** with *N*-methyl-L-prolinol (**4**), a global deprotection of alkoxylation product **2** in MsOH/AcOH, followed by the acrylamide warhead installation employing acrylic anhydride afforded GDC-6036 free base (**9**) in 76% yield over three steps. Finally, salt formation of the free base in methyl ethyl ketone (MEK) produced GDC-6036 adipate (**1**)[45] in 78% yield with <0.1% atropisomer of the API as ascertained by HPLC analysis (Scheme 7).

Scheme 7. Endgame Synthesis of GDC-6036 (1)

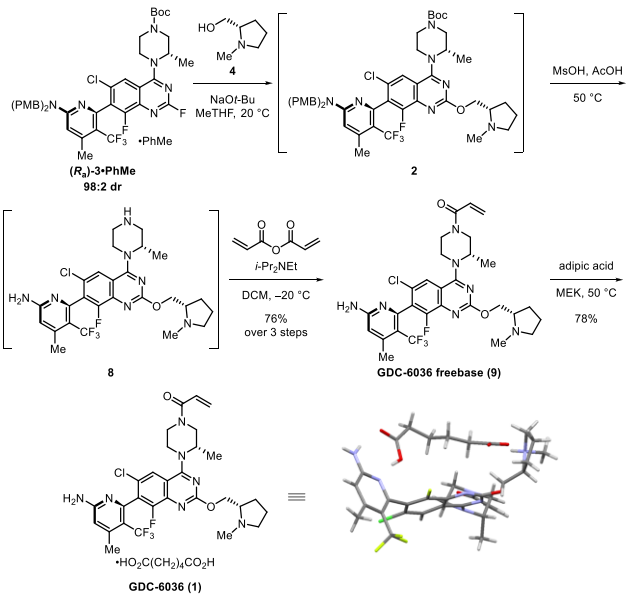

CONCLUSIONS

We have developed an asymmetric synthesis of a potent KRAS G12C inhibitor GDC-6036 (**1**) involving a highly atroposelective Negishi coupling of aminopyridine **5** and quinazoline organozinc species **6b**. The combination of HTE and statistical modeling led to the identification of an optimized Walphos ligand **W057-2**, which generated the coupling product in 85% assay yield with 92:8 atroposelectivity. The desired Negishi product (R_a)-**3** was isolated in 67% yield with 98:2 selectivity

https://doi.org/10.1021/jacs.2c09917
J. Am. Chem. Soc. 2022, 144, 20955−20963

by crystallization. A subsequent telescoped reaction sequence of alkoxylation, global deprotection, and acrylamide formation, followed by adipate salt formation, furnished GDC-6036 (**1**). Overall, GDC-6036 (**1**) was synthesized from starting materials pyridine **5** and quinazoline **6** in a 40% yield without the use of any preparative *chromatographic* purification or salt resolution, and the key reactions were demonstrated at >10 g scale.[46,47] The development of this first-generation asymmetric synthesis of GDC-6036 (**1**) provided the foundation for and significantly accelerated our next generation process development to support our KRAS G12C clinical development program. Furthermore, we assessed the generality of the atroposelective Negishi coupling with **W057-2** and demonstrated that even small changes in substrate structure significantly impact selectivity and yield. However, application of the MLR workflow to each substrate pairing allows for improvement in performance in most cases.

■ ASSOCIATED CONTENT

Supporting Information

The Supporting Information is available free of charge at https://pubs.acs.org/doi/10.1021/jacs.2c09917.

Experimental and computational details, spectral data, and copies of ^{1}H and ^{13}C NMR spectra (PDF)

Accession Codes

CCDC 2181275−2181276 contain the supplementary crystallographic data for this paper. These data can be obtained free of charge via www.ccdc.cam.ac.uk/data_request/cif, or by emailing data_request@ccdc.cam.ac.uk, or by contacting The Cambridge Crystallographic Data Centre, 12 Union Road, Cambridge CB2 1EZ, UK; fax: +44 1223 336033.

■ AUTHOR INFORMATION

Corresponding Authors

Haiming Zhang − *Department of Small Molecule Process Chemistry, Genentech, Inc., South San Francisco, California 94080, United States;* orcid.org/0000-0002-2139-2598; Email: zhang.haiming@gene.com

Matthew S. Sigman − *Department of Chemistry, University of Utah, Salt Lake City, Utah 84112, United States;* orcid.org/0000-0002-5746-8830; Email: sigman@chem.utah.edu

Authors

Jie Xu − *Department of Small Molecule Process Chemistry, Genentech, Inc., South San Francisco, California 94080, United States;* orcid.org/0000-0001-6424-1055

Samantha Grosslight − *Department of Chemistry, University of Utah, Salt Lake City, Utah 84112, United States*

Kyle A. Mack − *Department of Small Molecule Process Chemistry, Genentech, Inc., South San Francisco, California 94080, United States;* orcid.org/0000-0002-4986-4040

Sierra C. Nguyen − *Department of Small Molecule Process Chemistry, Genentech, Inc., South San Francisco, California 94080, United States*

Kyle Clagg − *Department of Small Molecule Process Chemistry, Genentech, Inc., South San Francisco, California 94080, United States;* orcid.org/0000-0001-6594-1950

Ngiap-Kie Lim − *Department of Small Molecule Process Chemistry, Genentech, Inc., South San Francisco, California 94080, United States;* orcid.org/0000-0002-3760-4874

Jacob C. Timmerman − *Department of Small Molecule Process Chemistry, Genentech, Inc., South San Francisco, California 94080, United States*

Jeff Shen − *Department of Small Molecule Process Chemistry, Genentech, Inc., South San Francisco, California 94080, United States*

Nicholas A. White − *Department of Small Molecule Process Chemistry, Genentech, Inc., South San Francisco, California 94080, United States;* orcid.org/0000-0001-5038-8865

Lauren E. Sirois − *Department of Small Molecule Process Chemistry, Genentech, Inc., South San Francisco, California 94080, United States;* orcid.org/0000-0002-1948-3749

Chong Han − *Department of Small Molecule Process Chemistry, Genentech, Inc., South San Francisco, California 94080, United States;* orcid.org/0000-0002-2863-3921

Francis Gosselin − *Department of Small Molecule Process Chemistry, Genentech, Inc., South San Francisco, California 94080, United States;* orcid.org/0000-0001-9812-4180

Complete contact information is available at: https://pubs.acs.org/10.1021/jacs.2c09917

Author Contributions

J.X. and S.G. contributed equally.

Notes

The authors declare no competing financial interest.

■ ACKNOWLEDGMENTS

We thank Jenny Wang, Zeenat Razvi, Karissa Cruz, Dr. Samuel Yang, Dr. Chris Crittenden, Dr. Jose Napolitano, Dr. Kenji Kurita, and Dr. David Russell for analytical support, Colin Masui for performing high-throughput experimentation, and Dr. Antonio DiPasquale for X-ray crystallographic support. S.G. and M.S.S. acknowledge the Center for High Performance Computing (CHPC) at the University of Utah for the support and resources provided, and Dr. Sean Ross and Dr. Jacob Werth for their helpful discussions. M.S.S. acknowledges financial support from NSF under the CCI Center for Computer Assisted Synthesis (CHE-1925607 and CHE−2202693).

■ REFERENCES

(1) Ostrem, J. M.; Peters, U.; Sos, M. L.; Wells, J. A.; Shokat, K. M. K-Ras(G12C) inhibitors allosterically control GTP affinity and effector interactions. *Nature* **2013**, *503*, 548−551.

(2) Wang, Y.; Kaiser, C. E.; Frett, B.; Li, H.-y. Targeting Mutant KRAS for Anticancer Therapeutics: A Review of Novel Small Molecule Modulators. *J. Med. Chem.* **2013**, *56*, 5219−5230.

(3) Gabizon, R.; London, N. Hitting KRAS When It's Down. *J. Med. Chem.* **2020**, *63*, 6677−6678.

(4) Chen, H.; Smaill, J. B.; Liu, T.; Ding, K.; Lu, X. Small-Molecule Inhibitors Directly Targeting KRAS as Anticancer Therapeutics. *J. Med. Chem.* **2020**, *63*, 14404−14424.

(5) Ryan, M. B.; Corcoran, R. B. Therapeutic strategies to target RAS-mutant cancers. *Nature Rev. Clin. Oncol.* **2018**, *15*, 709−720.

(6) Goebel, L.; Müller, M. P.; Goody, R. S.; Rauh, D. KRasG12C inhibitors in clinical trials: a short historical perspective. *RSC Med. Chem.* **2020**, *11*, 760−770.

(7) Lindsay, C. R.; Garassino, M. C.; Nadal, E.; Öhrling, K.; Scheffler, M.; Mazières, J. On target: Rational approaches to KRAS inhibition for treatment of non-small cell lung carcinoma. *Lung Cancer* **2021**, *160*, 152−165.

(8) Canon, J.; Rex, K.; Saiki, A. Y.; Mohr, C.; Cooke, K.; Bagal, D.; Gaida, K.; Holt, T.; Knutson, C. G.; Koppada, N.; Lanman, B. A.; Werner, J.; Rapaport, A. S.; San Miguel, T.; Ortiz, R.; Osgood, T.;

Sun, J.-R.; Zhu, X.; McCarter, J. D.; Volak, L. P.; Houk, B. E.; Fakih, M. G.; O'Neil, B. H.; Price, T. J.; Falchook, G. S.; Desai, J.; Kuo, J.; Govindan, R.; Hong, D. S.; Ouyang, W.; Henary, H.; Arvedson, T.; Cee, V. J.; Lipford, J. R. The clinical KRAS(G12C) inhibitor AMG 510 drives anti-tumour immunity. *Nature* **2019**, *575*, 217−223.

(9) Fell, J. B.; Fischer, J. P.; Baer, B. R.; Blake, J. F.; Bouhana, K.; Briere, D. M.; Brown, K. D.; Burgess, L. E.; Burns, A. C.; Burkard, M. R.; Chiang, H.; Chicarelli, M. J.; Cook, A. W.; Gaudino, J. J.; Hallin, J.; Hanson, L.; Hartley, D. P.; Hicken, E. J.; Hingorani, G. P.; Hinklin, R. J.; Mejia, M. J.; Olson, P.; Otten, J. N.; Rhodes, S. P.; Rodriguez, M. E.; Savechenkov, P.; Smith, D. J.; Sudhakar, N.; Sullivan, F. X.; Tang, T. P.; Vigers, G. P.; Wollenberg, L.; Christensen, J. G.; Marx, M. A. Identification of the Clinical Development Candidate MRTX849, a Covalent KRASG12C Inhibitor for the Treatment of Cancer. *J. Med. Chem.* **2020**, *63*, 6679−6693.

(10) Janes, M. R.; Zhang, J.; Li, L.-S.; Hansen, R.; Peters, U.; Guo, X.; Chen, Y.; Babbar, A.; Firdaus, S. J.; Darjania, L.; Feng, J.; Chen, J. H.; Li, S.; Li, S.; Long, Y. O.; Thach, C.; Liu, Y.; Zarieh, A.; Ely, T.; Kucharski, J. M.; Kessler, L. V.; Wu, T.; Yu, K.; Wang, Y.; Yao, Y.; Deng, X.; Zarrinkar, P. P.; Brehmer, D.; Dhanak, D.; Lorenzi, M. V.; Hu-Lowe, D.; Patricelli, M. P.; Ren, P.; Liu, Y. Targeting KRAS Mutant Cancers with a Covalent G12C-Specific Inhibitor. *Cell* **2018**, *172*, 578−589.

(11) Malhotra, S.; Xin, J.; Do, S.; Terrett, J. Fused Ring Compounds. U.S. Patent 20210230142, July 29, 2021.

(12) Kettle, J. G.; Bagal, S. K.; Bickerton, S.; Bodnarchuk, M. S.; Breed, J.; Carbajo, R. J.; Cassar, D. J.; Chakraborty, A.; Cosulich, S.; Cumming, I.; Davies, M.; Eatherton, A.; Evans, L.; Feron, L.; Fillery, S.; Gleave, E. S.; Goldberg, F. W.; Harlfinger, S.; Hanson, L.; Howard, M.; Howells, R.; Jackson, A.; Kemmitt, P.; Kingston, J. K.; Lamont, S.; Lewis, H. J.; Li, S.; Liu, L.; Ogg, D.; Phillips, C.; Polanski, R.; Robb, G.; Robinson, D.; Ross, S.; Smith, J. M.; Tonge, M.; Whiteley, R.; Yang, J.; Zhang, L.; Zhao, X. Structure-Based Design and Pharmacokinetic Optimization of Covalent Allosteric Inhibitors of the Mutant GTPase KRASG12C. *J. Med. Chem.* **2020**, *63*, 4468−4483.

(13) Christie, G. H.; Kenner, J. The molecular configurations of polynuclear aromatic compounds. Part I. The resolution of γ-6:6′-dinitro- and 4:6:4′:6′-tetranitro-diphenic acids into optically active components. *J. Chem. Soc. Trans.* **1922**, *121*, 614−620.

(14) Bringmann, G.; Price Mortimer, A. J.; Keller, P. A.; Gresser, M. J.; Garner, J.; Breuning, M. Atroposelective Synthesis of Axially Chiral Biaryl Compounds. *Angew. Chem., Int. Ed.* **2005**, *44*, 5384−5427.

(15) Alkorta, I.; Elguero, J.; Roussel, C.; Vanthuyne, N.; Piras, P. Chapter 1 - Atropisomerism and Axial Chirality in Heteroaromatic Compounds. In *Advances in Heterocyclic Chemistry*; Katritzky, A., Ed.; Academic Press, 2012; Vol. *105*, pp 1−188.

(16) Zask, A.; Murphy, J.; Ellestad, G. A. Biological Stereoselectivity of Atropisomeric Natural Products and Drugs. *Chirality* **2013**, *25*, 265−274.

(17) Cherney, A. H.; Kadunce, N. T.; Reisman, S. E. Enantioselective and Enantiospecific Transition-Metal-Catalyzed Cross-Coupling Reactions of Organometallic Reagents to Construct C-C Bonds. *Chem. Rev.* **2015**, *115*, 9587−9652.

(18) Cheng, D.-J; Shao, Y.-D. Advances in the Catalytic Asymmetric Synthesis of Atropisomeric Hexatomic *N*-Heterobiaryls. *Adv. Synth. Catal.* **2020**, *362*, 3081−3099.

(19) Cheng, J. K.; Xiang, S.-H.; Li, S.; Ye, L.; Tan, B. Recent Advances in Catalytic Asymmetric Construction of Atropisomers. *Chem. Rev.* **2021**, *121*, 4805−4902.

(20) Kang, H.; Lee, Y. E.; Reddy, P. V. G.; Dey, S.; Allen, S. E.; Niederer, K. A.; Sung, P.; Hewitt, K.; Torruellas, C.; Herling, M. R.; Kozlowski, M. C. Asymmetric Oxidative Coupling of Phenols and Hydroxycarbazoles. *Org. Lett.* **2017**, *19*, 5505−5508.

(21) Tian, M.; Bai, D.; Zheng, G.; Chang, J.; Li, X. Rh(III)-Catalyzed Asymmetric Synthesis of Axially Chiral Biindolyls by Merging C-H Activation and Nucleophilic Cyclization. *J. Am. Chem. Soc.* **2019**, *141*, 9527−9532.

(22) Shen, D.; Xu, Y.; Shi, S.-L. A Bulky Chiral *N*-heterocyclic Carbene Palladium Catalyst Enables Highly Enantioselective Suzuki-Miyaura Cross-Coupling Reactions for the Synthesis of Biaryl Atropisomers. *J. Am. Chem. Soc.* **2019**, *141*, 14938−14945.

(23) Yang, H.; Sun, J.; Gu, W.; Tang, W. Enantioselective Cross-Coupling for Axially Chiral Tetra-ortho-Substituted Biaryls and Asymmetric Synthesis of Gossypol. *J. Am. Chem. Soc.* **2020**, *142*, 8036−8043.

(24) For a recent example of atroposelective C−N bond formation for the synthesis of *N*-aryl heteroaryls, see: Zhang, P.; Wang, X.-M.; Xu, Q.; Guo, C.-Q.; Wang, P.; Lu, C.-J.; Liu, R.-R. Enantioselective Synthesis of Atropisomeric Biaryls by Pd-Catalyzed Asymmetric Buchwald-Hartwig Amination. *Angew. Chem., Int. Ed.* **2021**, *60*, 21718−21722.

(25) For a recent example of atroposelective N−N bond formation to construct nitrogen-rich heterocycles, see: Chen, K.-W.; Chen, Z.-H.; Yang, S.; Wu, S.-F.; Zhang, Y.-C.; Shi, F. Organocatalytic Atroposelective Synthesis of N-N Axially Chiral Indoles and Pyrroles by De Novo Ring Formation. *Angew. Chem., Int. Ed.* **2022**, *61*, No. e202116829.

(26) For the first atroposelective Negishi coupling, see: Genov, M.; Fuentes, B.; Espinet, P.; Pelaz, B. Asymmetric Negishi reaction for sterically hindered couplings: synthesis of chiral binaphthalenes. *Tetrahedron: Asymmetry* **2006**, *17*, 2593−2595.

(27) Genov, M.; Almorín, A.; Espinet, P. Microwave assisted asymmetric Suzuki-Miyaura and Negishi cross-coupling reactions: synthesis of chiral binaphthalenes. *Tetrahedron: Asymmetry* **2007**, *18*, 625−627.

(28) For another rare example of atroposelective Negishi coupling, see: Patel, N. D.; Sieber, J. D.; Tcyrulnikov, S.; Simmons, B. J.; Rivalti, D.; Duvvuri, K.; Zhang, Y.; Gao, D. A.; Fandrick, K. R.; Haddad, N.; Lao, K. S.; Mangunuru, H. P. R.; Biswas, S.; Qu, B.; Grinberg, N.; Pennino, S.; Lee, H.; Song, J. J.; Gupton, B. F.; Garg, N. K.; Kozlowski, M. C.; Senanayake, C. H. Computationally Assisted Mechanistic Investigation and Development of Pd-Catalyzed Asymmetric Suzuki-Miyaura and Negishi Cross-Coupling Reactions for Tetra-ortho-Substituted Biaryl Synthesis. *ACS Catal.* **2018**, *8*, 10190−10209.

(29) Negishi, E.-i.; Zeng, X.; Tan, Z.; Qian, M.; Hu, Q.; Huang, Z. Carbon-Carbon Bond Forming Reactions Mediated by Organozinc Reagents. In *Metal-Catalyzed Cross-Coupling Reactions*, 2nd ed.; de Meijere, A.; Diederich, F., Eds.; Wiley-VCH: Weinheim, 2004; pp 815−889.

(30) Negishi, E.-i. Magical Power of Transition Metals: Past, Present, and Future. *Angew. Chem., Int. Ed.* **2011**, *50*, 6738−6764.

(31) Sturm, T.; Weissensteiner, W.; Spindler, F. A novel class of ferrocenyl-aryl-based diphosphine ligands for Rh- and Ru-catalysed enantioselective hydrogenation. *Adv. Synth. Catal.* **2003**, *345*, 160−164.

(32) Wang, Y.; Strum, T.; Steurer, M.; Arion, V. B.; Mereiter, K.; Spindler, F.; Weissensteiner, W. Synthesis, Coordination Behavior, and Use in Asymmetric Hydrogenations of Walphos-Type Ligands. *Organometallics* **2008**, *27*, 1119−1127.

(33) Sigman, M. S.; Harper, K. C.; Bess, E. N.; Milo, A. The Development of Multidimensional Analysis Tools for Asymmetric Catalysis and Beyond. *Acc. Chem. Res.* **2016**, *49*, 1292−1301.

(34) At the outset of our investigation, we attempted the conversion of both pyridine and quinazoline bromides **5** and **6** to their corresponding organozinc species by metal−halogen exchange with *i*-PrMgCl·LiCl or *n*-BuLi followed by $ZnCl_2$ quench. The metal−halogen exchange of bromopyridine **5** turned out to be difficult, resulting in either low conversion of the starting material **5** or decomposition of the corresponding organometallic intermediates. The metal−halogen exchange of bromoquinazoline **6** with *n*-BuLi afforded a much less stable organolithium species than the corresponding aryl Grignard intermediate, thus was not extensively studied.

https://doi.org/10.1021/jacs.2c09917
J. Am. Chem. Soc. 2022, 144, 20955−20963

(35) Zahrt, A. F.; Athavale, S. V.; Denmark, S. E. Quantitative Structure-Selectivity Relationships in Enantioselective Catalysis: Past, Present, and Future. *Chem. Rev.* **2020**, *120*, 1620−1689.
(36) Walphos ligand **W022-1** containing norbornyl substituents is a mixture of four diastereomers with each having its own unique molecular features; therefore, it is not included in the multivariate linear regression model development.
(37) Santiago, C.; Gou, J.-Y.; Sigman, M. S. Predictive and Mechanistic Multivariate Linear Regression Models for Reaction Development. *Chem. Sci.* **2018**, *9*, 2398−2412.
(38) Durand, D. J.; Fey, N. Computational Ligand Descriptors for Catalyst Design. *Chem. Rev.* **2019**, *119*, 6561−6594.
(39) Jover, J.; Fey, N.; Harvey, J. N.; Lloyd-Jones, G. C.; Orpen, A. G.; Owen-Smith, G. J. J.; Murray, P.; Hose, D. R. J.; Osborne, R.; Purdie, M. Expansion of the Ligand Knowledge Base for Chelating P,P-Donor Ligands (LKB-PP). *Organometallics* **2012**, *31*, 5302−5306.
(40) Zhao, S.; Gensch, T.; Murray, B.; Niemeyer, Z. L.; Sigman, M. S.; Biscoe, M. R. Enantiodivergent Pd-catalyzed C-C bond formation enabled through ligand parameterization. *Science* **2018**, *362*, 670−674.
(41) Reed, A. E.; Weinstock, R. B.; Weinhold, F. Natural population analysis. *J. Chem. Phys.* **1985**, *83*, 735−746.
(42) Gómez-Suárez, A.; Nelson, D. J.; Nolan, S. P. Quantifying and understanding the steric properties of *N*-heterocyclic carbenes. *Chem. Commun.* **2017**, *53*, 2650−2660.
(43) DiPasquale, A. G. *CSD Communications* **2022**, CCDC 2181276.
(44) The HTS screening training set used for **7c−e** included Walphos **W037-1**. All other ligands within the training set were kept the same.
(45) DiPasquale, A. G. *CSD Communications* **2022**, CCDC 2181275.
(46) The isolation and purification of atropisomeric KRAS molecules proved to be highly challenging even by means of chromatographic separation. For an example, see: Nikitidis, G.; Carlsson, A.-C. C.; Karlsson, S.; Campbell, A. D.; Cook, C.; Dai, K.; Emtenäs, H.; Jonson, A. C.; Leek, H.; Malmgren, M.; Moravčík, Š.; Pithani, S.; Tatton, M. R.; Zhao, H.; Öhlén, K. Synthetic and Chromatographic Challenges and Strategies for Multigram Manufacture of $KRAS^{G12C}$ Inhibitors. *Org. Process Res. Dev.* **2022**, *26*, 710−729.
(47) For a recent example of synthesis of an atropisomeric KRAS molecule via salt resolution, see: Douglas, J. J.; Tatton, M. R.; de Bruin, D.; Buttar, D.; Cook, C.; Dai, K.; Ferrer, C.; Leslie, K.; Morrison, J.; Munday, R.; Ronson, T. O.; Zhao, H. Exploration of a Nitromethane-Carbonylation Strategy during Route Design of an Atropisomeric $KRAS^{G12C}$ Inhibitor. *J. Org. Chem.* **2022**, *87*, 2075−2086.

https://doi.org/10.1021/jacs.2c09917
J. Am. Chem. Soc. 2022, 144, 20955−20963